Check for updates

A novel highly selective electrochemical chlorobenzene sensor based on ternary oxide RuO$_2$/ZnO/TiO$_2$ nanocomposites

Md. Mahmud Alam, [a] Muhammad Zobayer Bin Mukhlish,[a] Ayesha Tazrin,[a] Nahida Akter Jui,[a] Abdullah M. Asiri, [bc] Mohammed M. Rahman, [bc] Md. Akhtarul Islam[a] and Md. Tamez Uddin [*a]

A novel electrochemical (EC) chlorobenzene (CBZ) sensor was fabricated using a ternary oxide RuO$_2$/ZnO/TiO$_2$ nanocomposite (NC)-decorated glassy carbon electrode (GCE). The nanoparticles (NPs) were synthesized by a wet-chemical method and characterized by X-ray photoelectron spectroscopy (XPS), powder X-ray diffraction (XRD), field emission scanning electron microscopy (FESEM), energy-dispersive X-ray spectroscopy (EDS), and ultraviolet-visible (UV-vis) spectroscopy. The synthesized RuO$_2$/ZnO/TiO$_2$ NC was layered as thin film on a GCE with Nafion (5% suspension in ethanol) adhesive, and the as-prepared sensor was subjected to CBZ analysis using an electrochemical approach. The calibration of the proposed CBZ sensor was executed with a linear relation of current *versus* concentration of CBZs known as the calibration curve. The sensitivity (32.02 μA μM^{-1} cm^{-2}) of the CBZ sensor was calculated from the slope of the calibration curve by considering the active surface area of the GCE (0.0316 cm^2). The lower detection limit (LD; 98.70 $\pm$ 4.90 pM) was also calculated at a signal-to-noise ratio of 3. Besides these, the response current followed a linear relationship with the concentration of chlorobenzene and the linear dynamic range (LDR) was denoted in the range of 0.1 nM to 1.0 μM. Moreover, the CBZ sensor was found to exhibit good reproducibility, reliability, stability, and fast response time. Finally, the sensing mechanism was also discussed with the energy-band theory of ternary doped semiconductor materials. The sensing activity of the proposed sensor was significantly enhanced due to the combined result of depletion layer formation at the heterojunction of RuO$_2$/ZnO/TiO$_2$ NCs as well as the activity of RuO$_2$ NPs as oxidation catalysts. The proposed CBZ sensor probe based on ternary oxide RuO$_2$/ZnO/TiO$_2$ NCs was developed with significant analytical parameters for practical application in monitoring the environmental pollutants of CBZs for the safety of environmental fields on a large scale.

1. Introduction

Aromatic chlorobenzene (CBZ) compounds are commonly used as raw materials, intermediates and solvents in insecticides, pesticides, pharmaceuticals, printing, dyeing, leather, and electronics industries.[1] All the chlorobenzenes used in pesticides and insecticides are directly released into soil during their application, and they enter the food chain *via* leaching of soil by rainwater. Therefore, the use of agrochemicals formulated with chlorobenzenes (pesticides and insecticides) is responsible for direct contamination of the environment. Besides this, the incomplete incineration of municipal, industrial and medical wastes is another important source of the release of CBZs into the environment.[2,3] As a result, the chlorinated volatile organic compounds from various stationary sources have great impact on environment due to its high toxicity.[4] Therefore, CBZs are considered the hazardous environmental pollutants.[5,6] As a result, there is a potential risk of accumulation of CBZs in human beings *via* the food chain. Consequently, this may cause teratogenesis, cancer, and mutagenesis and can badly affect the central nervous system and cause damage as reported previously.[7] In addition, it may also cause copious symptoms such as headache, numbness, sleepiness, vomiting, liver and kidney damage.[8] Therefore, the United States Environmental Protection Agency (EPA) has ranked CBZs as priority toxic pollutants.[9] Therefore, a reliable analytical method to determine CBZs in the environment is obviously very important.

[a] *Department of Chemical Engineering and Polymer Science, Shahjalal University of Science and Technology, Sylhet 3100, Bangladesh. E-mail: mtuddin_cep@yahoo. com; mtuddin-cep@sust.edu*

[b] *Department of Chemistry, King Abdulaziz University, Faculty of Science, P.O. Box 80203, Jeddah 21589, Saudi Arabia*

[c] *Center of Excellence for Advanced Materials Research (CEAMR), King Abdulaziz University, P.O. Box 80203, Jeddah 21589, Saudi Arabia*

Up to date, chlorobenzenes are determined quantitatively applying different conventional techniques such as gas chromatography,[8] mass spectrometry,[10] HPLC,[11] ion mobility spectrometry,[12] and other integrated methods. However, these techniques face different critical limitations including complicated fabrication, high cost, time consumption in sample pretreatment including separation and the prolonged data analysis. Over the past decades, electrochemical (EC) methods have received excessive attention in various diagnoses including clinical,[13–15] environmental,[16,17] biological,[18] pharmaceutical, and quality control during food processing.[19] Among the EC methods, the electrochemical approach has drawn significant attention of researchers due to its high sensitivity, good selectivity, inexpensive instruments, ease of operation, simple pretreatment of samples, and faster analysis. To improve the sensitivity and avoid the multi-selectivity, the electrodes have been modified with various semi-conductive metal oxides such as ZnO,[20–22] Cr_2O_3,[23] SnO_2,[24] WO_3,[25] and Co_3O_4 to detect numerous toxic chemicals and biochemicals.[26] In the recent years, few research studies based on semi-conductive metal oxides have been reported for the reliable detection of CBZs. As reported previously, Pt-decorated ZnO NCs,[27] Au-decorated $ZnFe_2O_4$ yolk–shell spheres,[28] In_2O_3 nano-rods,[29] Pd NPs on porous ZnO nano-plates,[30] and coral-like SnO_2 nanostructures[31] have been reported as efficient sensing mediators for the reliable detection of CBZs. Besides this, FeO/CdO nanocubes and MCM-41 material-decorated GCEs have performed potentially to detect CBZs in an electrochemical approach.[32,33]

Among semiconductor metal oxides, zinc oxide (ZnO) has attracted great attention as a promising sensing material owing to its outstanding stability, non-toxicity, electrical properties, photosensitivity, EC activities, high electron communicating features, and so on.[34–37] Therefore, as an effectual sensing material, ZnO has been used previously to detect xanthine,[38] hydrazine,[39] 3-methoxyphenol,[40] 4-aminophenol,[41] and 4-nitrophenol.[42] However, most of these research works have been executed to detect toxic chemicals in the gaseous phase. Furthermore, the sensitivity and selectivity of these modified electrodes are not satisfactory enough for real-time applications. In this context, the modification of electrodes utilizing two or multiple semi-conductive metal oxide nanocomposites could be an effective way to enhance the selectivity as well as sensitivity of the EC sensors. In addition, any change in interfacial resistance due to the formation of a heterojunction results in improved performance of sensors.[43]

Composite metal oxides have already been utilized for the reliable and selective detection of numerous toxicants in the gaseous phase, such as ZnO/SnO_2 nanofibers for ethanol,[44] ZnO/Cr_2O_3 nanorods and ZnO/In_2O_3 nanofibers for trimethylamine,[45,46] V_2O_5 doped ZnO NCs for phenylhydrazine,[17] MgO/ZnO composite for H_2O_2,[47] and RuO_2/ZnO NCs for 2-nitrophenol[16] as reported earlier. Similarly, TiO_2 is another n-type semiconductor with a wide optical band gap, and it has good stability and opto-electro-chemical properties.[48] TiO_2, due to its multiple properties, has already been tested as an excellent sensor material to sense tetracycline,[49] hydrogen,[50] glucose,[51] formaldehyde,[52] uric acid[53] and hydrogen peroxide.[54,55] Besides

this, RuO_2 exhibits brilliant electronic and electro-catalytic properties.[56] As a result, RuO_2-based nanomaterials have been applied as supercapacitors,[57] electrodes for oxygen and chlorine production, water splitting,[58,59] CO oxidation[60] and HCl oxidation[61,62] as testified previously. Here, the incorporation of RuO_2 into a ZnO/TiO_2 nanostructured material was employed as a great deal of consideration due to its chemical, structural, physical, and optical properties in terms of large active surface area, high stability, and high porosity.[63] These properties are directly dependent on the structural morphology of the reactant precursors for making the ternary $RuO_2/ZnO/TiO_2$ materials a basic medium at low temperatures. This $RuO_2/ZnO/TiO_2$ material was synthesized by a facile solution method using reducing agents. This technique has several advantages including facile preparation, accurate control of reactant temperature, ease of handling, and one-step reaction. Optical, morphological, electrical, and chemical properties of the ternary $RuO_2/ZnO/TiO_2$ nanomaterial are of huge significance from the scientific aspect, compared to the counterpart ZnO, TiO_2, and RuO_2 nanomaterials. Non-stoichiometry, mostly oxygen vacancies, renders it the conducting nature in heterostructure materials.[64,65] The formation energy of oxygen vacancies in the semiconductor is very low and thus this defect forms eagerly, resulting in the increased conductivity of $RuO_2/ZnO/TiO_2$ materials compared to other pure materials. Ternary materials have also attracted considerable interest due to their potential applications including, optoelectronics, electro-analyses, selective detection assays, chemical sensor devices, hybrid-composites, electron field emission sources, biochemical detection, and surface-enhanced Raman scattering.[66,67] $RuO_2/ZnO/TiO_2$ materials offer improved performance due to the large active surface area, which increased the conductivity and current responses of the $RuO_2/ZnO/TiO_2$ NCs/Nafion/GCE assembly during the electrochemical investigation. It has been stated that ZnO, TiO_2 and RuO_2 have been applied as sensing mediators for the development of various toxic chemical sensors. In this context, combining ZnO, TiO_2 and RuO_2 metal oxides to form composite semiconductors would have a synergetic effect, which might improve the sensing performance of EC sensors. Thus, the investigation of the potentiality of $RuO_2/ZnO/TiO_2$ NCs as sensor materials would be of great scientific and technical interest. Furthermore, as far as we know, no EC sensor based on ternary oxide $RuO_2/ZnO/TiO_2$ NCs is yet reported for the detection of CBZs in a buffer medium.

In this approach, a novel EC sensor based on a wet-chemically prepared $RuO_2/ZnO/TiO_2$ NC-modified GCE was developed. Subsequently, the sensing performance of the projected sensor was investigated for the selective detection of chlorobenzenes. The I–V technique was employed to conduct all the experiments. To execute the analytical performances such as linear dynamic range (LDR), sensitivity and detection limit (DL) of the fabricated chlorobenzene sensor, a calibration curve was prepared by plotting current against chlorobenzene concentration. Then, the performance of the chlorobenzene sensor was investigated in detail.

2. Materials and methods

2.1. Chemicals and reagents

The TiO$_2$, ZnO and RuO$_2$ nanoparticles were synthesized using analytical grade titanium(IV) butoxide (Ti(OCH$_2$CH$_2$CH$_2$CH$_3$)$_4$), acetoxyzinc dihydrate (Zn(Ac)$_2$·2H$_2$O), and ruthenium trichloride trihydrate (RuCl$_3$·3H$_2$O) respectively, and these chemicals were obtained from Sigma Aldrich (Germany). To accomplish this study, the environmental toxins such as 1,4-dioxane, 3-chlorophenol, 2,4-dinitrophenol (2,4-DNP), chlorobenzene (CBZ), p-nitrophenol (p-NP), 4-nitrophenyl hydrazine (4-NPHyd), phenylhydrazine (PHyd), m-xylene, zimataldehyde, and pyridine were procured from Sigma-Aldrich and used as purchased. Besides this, Nafion (5% suspension in ethanol), and mono- and disodium phosphate were similarly acquired from Sigma Aldrich (Germany).

2.2. Synthesis of nanoparticles

2.2.1. Synthesis of TiO$_2$ NPs.
An efficient sol–gel technique was applied to prepare titanium oxide (TiO$_2$) NPs using titanium butoxide as a precursor following the procedure described elsewhere.[68] Following this typical method, 4 mL titanium butoxide was added into a 50 mL beaker containing a mixture of 2.6 mL acetic acid and 4.3 mL butanol. Then, 4 mL water was slowly added into the beaker and kept under continuous stirring to yield TiO$_2$ as a colloid form. After that, the resulting colloidal solution was kept under similar conditions for another 5 h. Finally, the obtained colloid was dried at 110 °C overnight and followed by calcination at 500 °C for 2 h. At the end, the calcined powder was ground and stored in an air-tight container.

2.2.2. Synthesis of ZnO NPs.
ZnO nanoparticles were prepared by a homogeneous precipitation technique using Zn(Ac)$_2$·2H$_2$O precursor and urea as a precipitating agent. In this wet-chemical method, a solution of 12.0 g urea and 3.12 g Zn(Ac)$_2$·2H$_2$O in 200.0 mL deionized water was taken in a 250.0 mL beaker and placed on a hot plate at 90 °C for 4 h with continuous stirring. A white precipitate of ZnO was obtained under vigorous mixing. Then, the mixture was kept under ambient conditions in the laboratory to settle down, and the a precipitate of ZnO was obtained. After that, the ZnO precipitate was separated from the aqueous medium and washed successively with deionized water. Then, it was kept inside an oven at 110 °C overnight to dry. The as-prepared dried particles were then ground into fine particles and annealed at 500 °C for 2 h. Finally, the annealed powder was further ground and stored in an air-tight container.

2.2.3. Synthesis of RuO$_2$/ZnO/TiO$_2$ ternary nanocomposites.
The RuO$_2$/ZnO/TiO$_2$ NCs containing different percentages of RuO$_2$ were prepared by an impregnation technique described previously,[69] keeping the weight ratio of TiO$_2$ and ZnO constant. According to the described impregnation method, a predetermined amount of RuCl$_3$·H$_2$O was dissolved in 50.0 mL deionized water in a 100 mL beaker. Then, 0.15 g of the prepared TiO$_2$ NPs and 0.15 g of ZnO NPs were dispersed into the RuCl$_3$·H$_2$O solution with continuous stirring for 4 h. At the same time, water was removed by evaporation to result in nanoparticles. Finally, the obtained nanoparticles were calcined in a muffle furnace at 500 °C for 2 h in the presence of atmospheric oxygen to result in the desired RuO$_2$/ZnO/TiO$_2$ NCs.

2.3. Characterizations of NPs

The phase crystallinity of the prepared NPs was investigated using a X-ray diffractometer (model 3040XPert PRO, Philips) at 2θ degree in the range of 10–80°. The mean size of the crystallite was calculated applying Scherrer's formula. X-ray photoelectron spectra (XPS) were recorded using a Thermo-Scientific spectrophotometer (Thermo Scientific K-Alpha KA1066 spectrometer) equipped with an Al-Kα X-ray excitation radiation source with a beam-spot size of 300.0 μm. Besides this, field emission scanning electron microscopy (FESEM; JSM-7600F, JEOL, Japan) equipped with an EDS was used to investigate the elemental analysis and surface morphology of RuO$_2$/ZnO/TiO$_2$ NCs. Moreover, a Keithley electrometer (6517A, USA) was applied as the central dominating equipment to supply constant potential for the exploration of the electrochemical behavior of the proposed sensor. The band gap energy of the prepared NPs was determined by measuring the UV-vis diffuse reflectance spectra (UV-vis DRS) of the NPs under ambient conditions. The UV-vis DRS was recorded by scanning the samples from 200 to 800 nm using a UV-vis-NIR spectrometer (LAMDA 750, Perki-nElmer, Inc, USA). Furthermore, Sintered PTFE was used as the standard reference.

2.4. Fabrication RuO$_2$/ZnO/TiO$_2$ NC-based sensor

The working electrode that is the key element of an EC sensor was produced by modifying a conventional GCE (surface area of 0.0316 cm^2) with a slurry of RuO$_2$/ZnO/TiO$_2$ NCs. To execute this modification task, the slurry was formulated by adding a suitable quantity of RuO$_2$/ZnO/TiO$_2$ NCs to ethanol. A thin film of RuO$_2$/ZnO/TiO$_2$ NCs was subsequently obtained by dropwise addition of the slurry on the active area of the GCE followed by drying under ambient conditions. A suspension containing 5% Nafion in ethanol was added to the RuO$_2$/ZnO/TiO$_2$ NC thin film in order to enhance the binding strength of the film. After adding Nafion binder, the film was kept in an oven at 35 °C to dry it again entirely. Finally, the desired electrochemical cell known as the sensor was assembled using a Keithley electrometer, where the modified GCE as RuO$_2$/ZnO/TiO$_2$ NCs/GCE and a Pt wire were connected using a Keithley electrometer in a series. It is noted that the assembled sensor was based on a two-electrode (working and counter) system. The performance of the recently developed EC sensor towards the analyte chlorobenzene was determined in a phosphate buffer solution. A number of chlorobenzene solutions of concentrations ranging from 0.1 mM to 0.1 nM were produced by diluting the 0.1 mM stock solution of chlorobenzene and used as the target analyte for the electrochemical characterization of the CBZ sensor. The response current was estimated applying a potential from 0.0 to +1.5 V. The pH and the volume of solution were kept fixed to 7 and 10 mL, respectively. A linear relation of current versus concentration of CBZs was executed to form the calibration

curve of CBZ sensor. The slope of calibration curve and surface area of GCE (0.0316 cm^2) were used to calculate the sensitivity of the CBZ sensor. Considering the maximum linear segment on the calibration curve, the linear dynamic range for CBZ detection was identified. Applying a signal-to-noise ratio of 3, the lower limit of the CBZ sensor was estimated. Equimolar concentrations of mono- and disodium phosphate were used to prepare a buffer medium of pH 7.0.

3. Results and discussions

3.1. Characterization of NPs

3.1.1. XRD analysis. The powder X-ray diffraction (XRD) analysis was performed on the synthesized NPs to identify the phase crystallinity and average crystal size of RuO$_2$/ZnO/TiO$_2$ NCs, as illustrated in Fig. 1. As perceived in Fig. 1(a), the diffracted peaks of pure TiO$_2$ at 2θ of $25.4°$, $37.7°$, $48°$, $53.8°$, $55.1°$ and $62.36°$ were ascribed to the crystallographic structure anatase phase TiO$_2$ and could be indexed as the (101), (004), (200), (105), (211), (204) and (103) planes, respectively. The observed diffraction peaks of TiO$_2$ were well matched with the values cited in the literature[70,71] and JCPDS no. 0078-2486. Besides this, the diffraction peaks for ZnO at $2\theta = 31.8°$, $34.5°$, $36.38°$, $47.6°$, $56.6°$ and $62.85°$ are exhibited in Fig. 1(c) and indexed as the (100), (002), (101), (102), (110), (103), and (112) planes, respectively, which were identified by JCPDS no. 0036-1451 and previously reported articles on ZnO.[72,73] Moreover, Fig. 1(b) shows the characteristic XRD pattern of RuO$_2$/ZnO/TiO$_2$ NCs and all the reflected lines were similar to the diffraction peaks of TiO$_2$, as shown in Fig. 1(a), and ZnO, as shown in Fig. 1(c). However, the peaks diffracted from the planes of RuO$_2$ in Fig. 1(b) did not appear clearly owing to the overlap of a more intense peak of ZnO. As anonymous XRD peaks were not perceived in Fig. 1(b), it can be confirmed that RuO$_2$/ZnO/TiO$_2$ NCs was prepared without any contamination. The mean crystallite size (D) of the prepared samples was estimated using Debye–Scherrer's formula[74] as follows:

$$D = (0.9\lambda)/(\beta \cos \theta) \qquad (1)$$

where λ is the wavelength of Cu Kα radiation ($\lambda = 1.5405$ Å), β is the full width at half maximum (FWHM) for the diffraction line under the consideration (radian) and θ is the diffraction angle (°). The value of θ for the ZnO (101) peak was $18.19°$ and the TiO$_2$ (101) peak was $12.7°$. The corresponding β values were estimated to be 0.30 and 0.43 for ZnO and TiO$_2$, respectively. From the XRD pattern of RuO$_2$/ZnO/TiO$_2$ NCs, as shown in Fig. 1(b), the crystallite sizes of the ZnO NPs at the (101) plane and TiO$_2$ NPs at the (101) plane were found as 27.86 and 18.93 nm, respectively, which were very close to pure ZnO (26.1 nm), as shown in Fig. 1(c), and TiO$_2$ (15.47 nm), as shown in Fig. 1(a) respectively.

3.1.2. XPS analysis. The XPS studies were executed on RuO$_2$/ZnO/TiO$_2$ NCs to explore the chemical compositions and oxidation states of the elements existing in the synthesized RuO$_2$/ZnO/TiO$_2$ NCs. The XPS survey spectra of RuO$_2$/ZnO/TiO$_2$ NCs shown in Fig. 2 demonstrated that the emissions of only
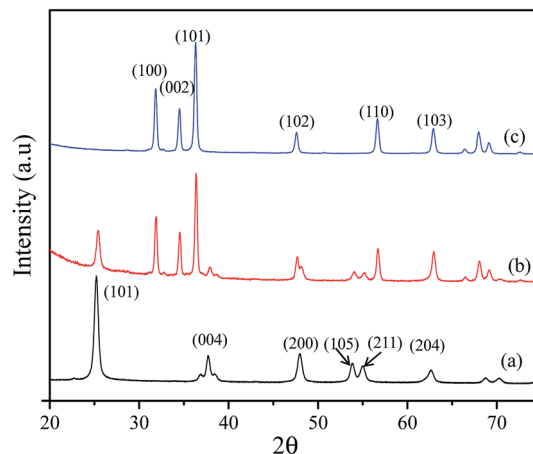

Fig. 1 Comparison of X-ray diffraction pattern of synthesized NPs. (a) XRD patterns of TiO$_2$ NPs, (b) the X-ray diffracted peaks of RuO$_2$/ZnO/TiO$_2$ NCs, and (c) resulted X-ray lines of ZnO NPs.

Zn, O, Ti, Ru and C were detected. The detected signal originated from the adsorbed carbon on the surface during the exposure of the NPs to the ambient atmosphere, which commonly exists for XPS. Any peak associated with the presence of impurity was not identified. Thus, the XPS study confirmed that the RuO$_2$/ZnO/TiO$_2$ samples were composed of only ZnO, TiO$_2$ and RuO$_2$ NPs.

The XPS high-resolution spectra of Ti 2p (Fig. 3(A)) displayed two peaks in the Ti 2p region: the first peak at 458.85 eV was assigned to Ti 2p$_{3/2}$ and the second peak at 464.50 eV was ascribed to Ti 2p$_{1/2}$. The distance between Ti 2p$_{1/2}$ and Ti 2p$_{3/2}$ peaks was 5.65 eV, which was a characteristic value of the Ti^{4+} ionization state as reported previously.[75,76] The distances between splitting Ti 2p$_{1/2}$ and Ti 2p$_{3/2}$ peaks have been stated as 5.73, 5.60, 5.66, and 6.13 eV for Ti^{2+}, Ti^{3+}, Ti^{4+} and metallic Ti^0, respectively.[76] This evidenced no contribution of reduced Ti^{3+} in the spectrum. The XPS spectra of Zn 2p (Fig. 3(B)) demonstrated two peaks at 1021.88 and 1044.98 eV, respectively, which were symmetric and originated from the spin-orbital splitting of the
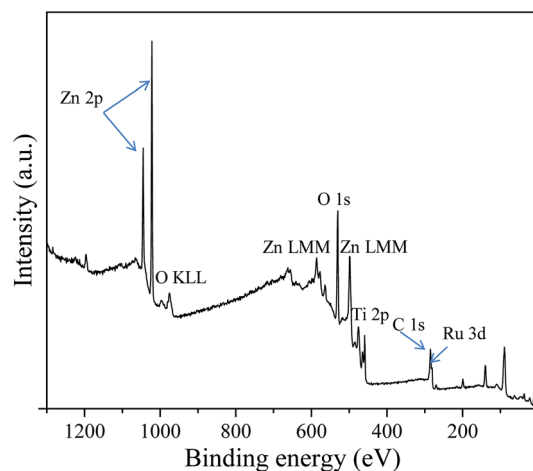

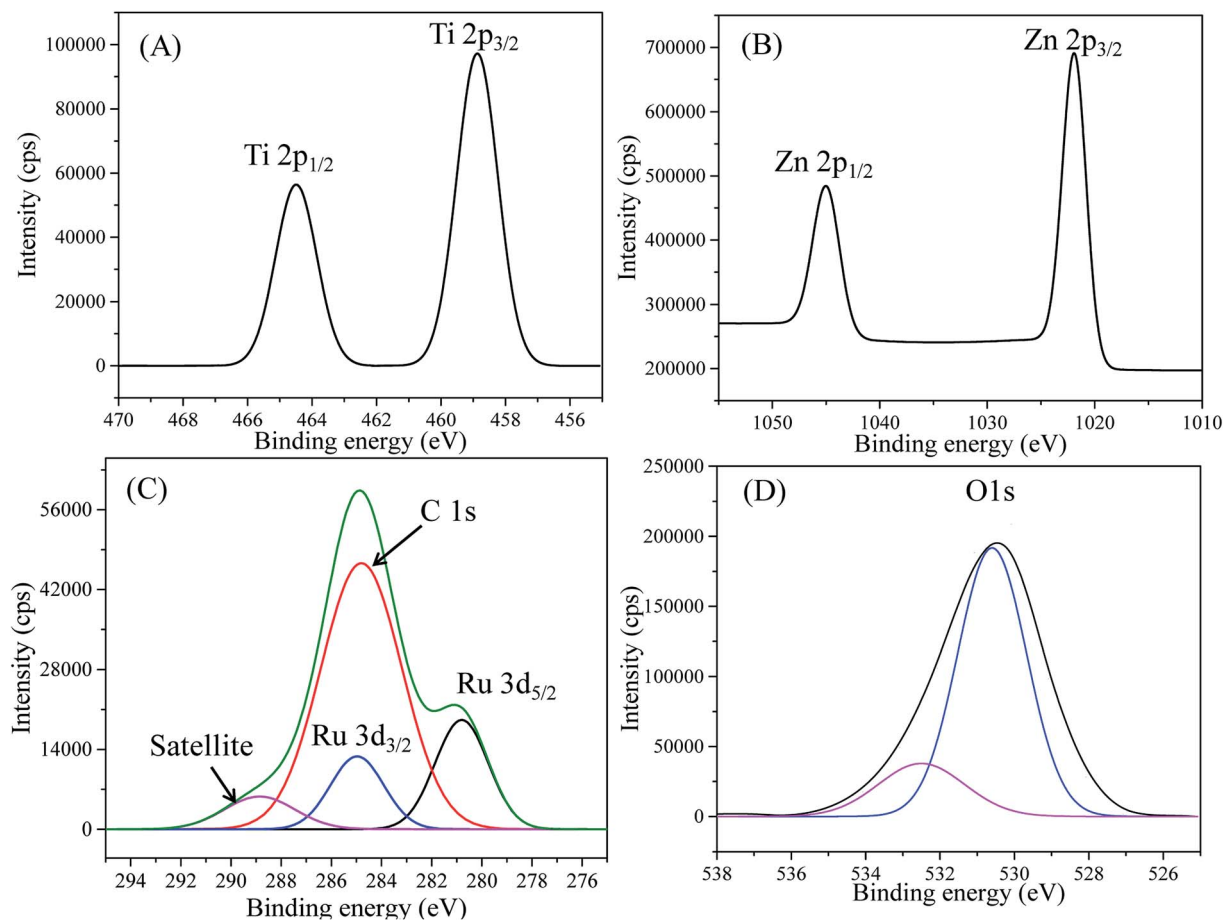**Fig. 2** XPS survey spectrum of RuO$_2$/ZnO/TiO$_2$ NCs.

Fig. 3 (A) High-resolution XPS spectra of Ti 2p, (B) Zn 2p level orbital, (C) C 1s + Ru 3d, and (D) O 1s orbit of RuO₂/ZnO/TiO₂ NCs.

Zn $2p_{3/2}$–Zn $2p_{1/2}$ core level states of Zn assigned to the lattice ZnO.[77] The distance (23.1 eV) between Zn $2p_{3/2}$ and Zn $2p_{1/2}$ peaks was similar to the standard reference value of ZnO.[78] These estimated values of the Zn 2p spectra confirmed the Zn^{2+} oxidation state of Zn in RuO₂/ZnO/TiO₂ NCs.[78,79]

Moreover, Fig. 3(C) revealed emission lines of the core-level Ru 3d orbit, which was the overlapped C 1s orbit as perceived. However, the deconvolution of the obtained Ru 3d level as in Fig. 3(C) resulted in three peaks for Ru $3d_{5/2}$, Ru $3d_{3/2}$ and C 1s. As illustrated in Fig. 3(C), the spin orbitals of Ru $3d_{5/2}$ and Ru $3d_{3/2}$ were located at 280.8 and 284.97 eV, respectively, and identified for Ru^{4+} cation existing in the synthesized NPs, as reported previously.[78,80] Furthermore, Fig. 3(D) displayed the O 1s orbital of RuO₂/ZnO/TiO₂ NCs, which was asymmetric indicating the several chemical states existing in the NCs. The deconvolution of the O 1s peak confirmed the two surface compositions of synthesized NCs. The most intense peak as shown in Fig. 3(D) was located at 530.5 eV and could be ascribed to lattice oxygen as Zn–O, Ti–O and Ru–O bonds in the prepared NCs.[81–84] However, the weaker peak at 532.5 eV was associated with oxygen in hydroxyl groups on the surface of NPs, *i.e.*, Ti–OH, Ru–OH and Zn–OH bonds.[84–86]

3.1.3. SEM and EDX analysis. The morphology of the surface of prepared nanomaterials is one of the key parameters that affect the sensing activity of the NPs as a sensing mediator. The RuO₂/ZnO/TiO₂ nanomaterials were investigated by FESEM, as presented in Fig. 4. The low- and high-magnification images of FESEM analysis shown in Fig. 4(A and B) revealed that the RuO₂/ZnO/TiO₂ nanomaterials were nanoparticles in shape with irregular size and aggregation. This similar evidence was found from the observation of EDS image, as revealed in Fig. 4(C). The elemental analysis as demonstrated in Fig. 4(D) confirmed the presence of Zn, Ti, Ru, and O only in the synthesized NCs and any peak was not identified for impurity. As perceived in Fig. 4(D), the elemental compositions of RuO₂/ZnO/TiO₂ NCs were 26.23% O, 3.32% Ti, 62.26% Zn, and 8.19% Ru as weight. The average size of NPs was calculated as 32.5 nm in the range of 20.0–40.0 nm. The size distribution of NPs was calculated from the SEM image and presented in Fig. 4(E).

3.1.4. UV-vis DRS analysis. The UV-vis DRS was employed to inspect the optical property of the as-synthesized NPs. The UV-vis DRS spectra of NPs are displayed in Fig. 5(A). As illustrated in Fig. 5(A), the TiO₂ NPs and ZnO NPs exhibited the characteristic spectra with fundamental sharp absorption edges at 382 and 370 nm, respectively. The direct optical band gap energy (E_g) of the semiconductor is generally determined following the equation $\alpha(h\nu) = A(h\nu - E_g)^{1/2}$, where α, ν, and A are denoted as the absorption coefficient, light frequency, and
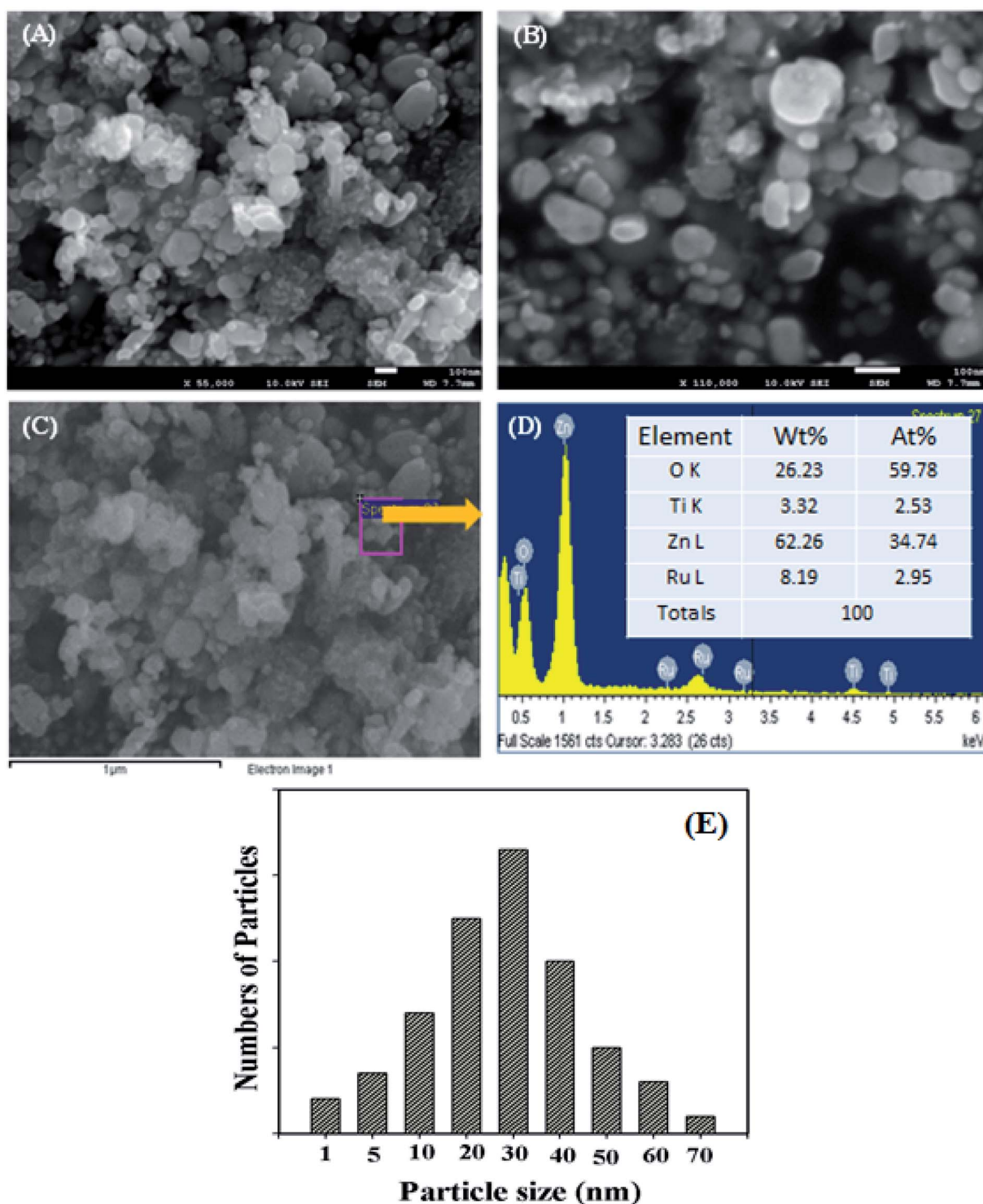
Element	Wt%	At%
O K	26.23	59.78
Ti K	3.32	2.53
Zn L	62.26	34.74
Ru L	8.19	2.95
Totals	100	

Fig. 4 (A and B) Low- and high-magnification FESEM images of RuO_2/ZnO/TiO_2 NPs, (C) image of EDS, (D) the elemental compositions of RuO_2/ZnO/TiO_2 NCs as weight and atomic percentages, and (E) size distribution of NPs.

constant, respectively.[87] The value of E_g is obtained by extrapolating a straight line to the abscissa axis, where $\alpha = 0$.[88] The Kubelka–Munk theory gives a relation between α and remission function $F(R)$, which is defined as $\alpha/s = F(R) = (1R)^2/(2R)$, where s is the scattering coefficient and R is the diffused reflectance.[89]

Thus, the values of E_g of the prepared samples were obtained from intercepts of the tangents of the plot of $(F(R)h\nu)^2$ *versus* $(h\nu)$. The values of E_g of TiO_2, ZnO and RuO_2/ZnO/TiO_2 were estimated to be 3.22, 3.32 and 3.25 eV, respectively, as shown in Fig. 5(B).
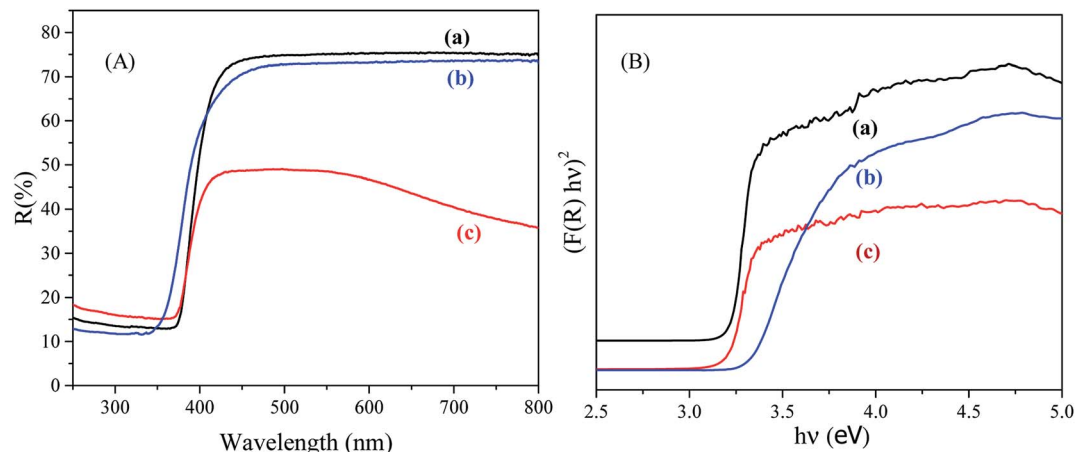
Fig. 5 (A) UV-vis DRS and (B) $(F(R)h\nu)^2$ *versus* $h\nu$ plot of (a) TiO_2, (b) ZnO and (c) 1 wt% ternary $RuO_2/ZnO/TiO_2$ NCs.

3.2. Analytical performance of $RuO_2/ZnO/TiO_2$ NC-based sensors

The sensing characterization of the proposed ternary $RuO_2/ZnO/TiO_2$ NC-based EC sensor was investigated by applying the current–voltage (I–V) technique. The EC sensor was developed by modifying a GCE with $RuO_2/ZnO/TiO_2$ NCs as a thin layer of film that served as the working electrode, while a Pt wire functioned as the counter electrode to assemble the sensor. One of the requirements of this study was the stability of NPs on the GCE. Therefore, few drops of Nafion adhesive were added on the surface of the modified GCE, which enhanced the stability of NPs layer on the GCE during electrochemical investigation and increased the conductance of the assembled working electrode due to the conductive nature of the Nafion co-polymer. As a result, the assembled sensor experienced intense electrochemical responses as the comparable statement has been reported previously in the detection of various chemicals and bio-chemicals in an electrochemical approach.[16,90,91] In

electrochemical detection, the observed current was assessed on the surface of a thin layer of NCs on the GCE and the delay time in electrometer was constantly set as 1 s throughout the investigation. To explore the selectivity of the assembled sensor, the different analytes with a concentration of 0.1 μM in a phosphate buffer of pH 7.0 were analyzed at a potential ranging from 0 to +1.5 V, as illustrated in Fig. 6(A). As demonstrated in Fig. 6(A), the chlorobenzene (CBZ) exhibited superior electrochemical response to 1,4-dioxane, 2,4-dinitrophenol, 3-chlorophenol, 4-nitrophenylhydrazine, *m*-xylol, phenylhydrazine, *p*-nitrophenol, pyridine, zimtaldehyde. Therefore, considering the highest electrochemical reactivity of CBZs toward the sensor assembly, it was denoted as the selective chemical to $RuO_2/ZnO/TiO_2$ NCs on the GCE. The consequence of the compositions of $RuO_2/ZnO/TiO_2$ NCs in electrochemical sensing of CBZs was studied to explore the optimum composition of NCs as shown in Fig. 6(B). As observed in Fig. 6(B), the ternary nanoparticles of 1% $RuO_2/ZnO/TiO_2$ showed high electrochemical sensing performance
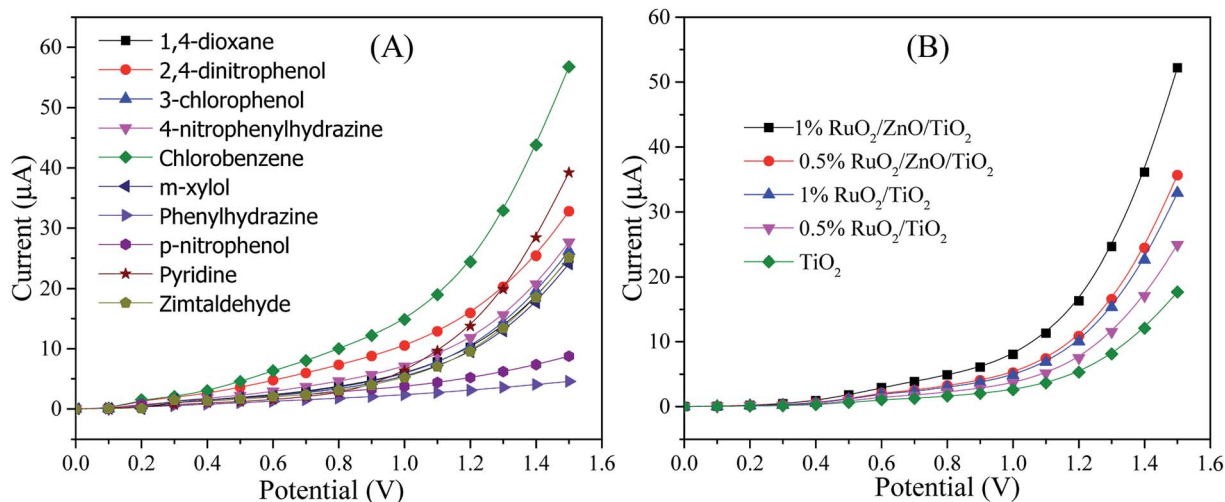

Fig. 6 Performance optimization of the $RuO_2/ZnO/TiO_2/GCE$-based chlorobenzene sensor. (A) Electrochemical investigation of toxic chemicals to execute the selectivity of the sensor at 0.1 μM in a buffer phase of pH 7.0, and (B) the control experiments to optimize the composition of ternary $RuO_2/ZnO/TiO_2$ NCs as CBZ sensing mediators.
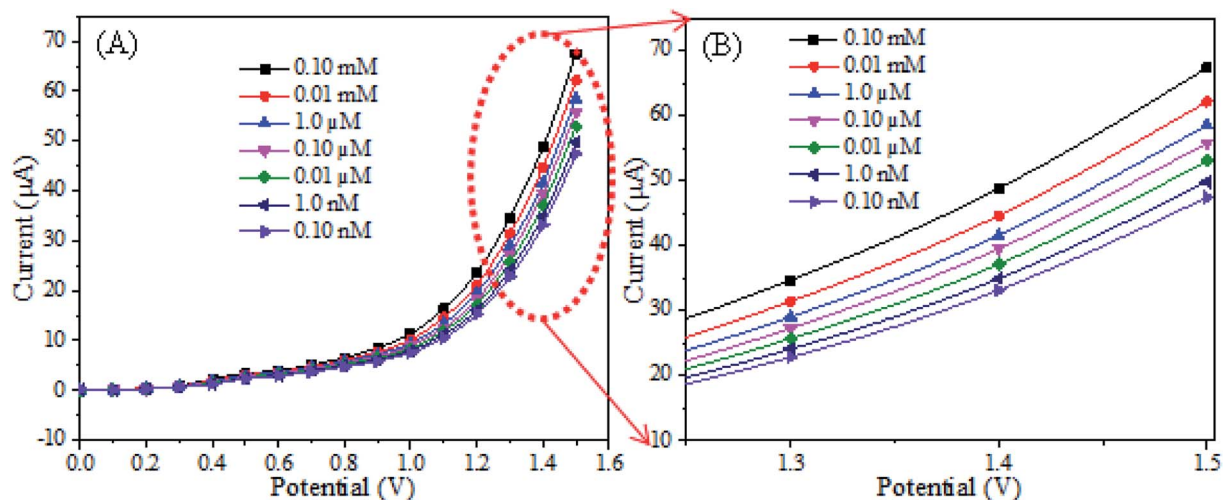
Fig. 7 (A) Typical current–voltage responses of the fabricated sensor at different concentrations of CBZs, and (B) magnified electrochemical responses of the sensor at different CBZ concentrations in the range from 1.2 to 1.5 V.

among the other compositions in analysis of CBZs at 0.1 μM and a potential of 0 to +1.5 V in a buffer phase of pH 7.0. This higher electrochemical response could be ascribed to the combined effects of RuO_2, ZnO and TiO_2 NPs. The mechanism of improved response of the proposed sensor based on 1% RuO_2/ZnO/TiO_2/GCE would be discussed in detail in the subsequent section.

Then, the RuO_2/ZnO/TiO_2 NPs/GCE sensor was subjected to analysis of CBZ solution based on the concentration ranging from 0.1 nM to 0.1 mM in a buffer phase as explored in Fig. 7(A). As presented in Fig. 7(A), the electrochemical responses of CBZs with the assembled sensor were enriched with the increase in chlorobenzene concentrations and distinguishable over the concentration range. The distinguishable responses of the proposed sensor towards different concentrations of CBZs were further confirmed by presenting an enlarged view of Fig. 7(A), as shown in Fig. 7(B). Similar tendencies of electrochemical

responses to detect different toxicants have been reported earlier.[16,92–94] This result reflected that the conductivity of the fabricated RuO_2/ZnO/TiO_2 NC-modified electrode increased with the enrichment of CBZ concentration, as excess free electrons were provided to the conduction bands of ZnO and TiO_2 NPs in the synthesized RuO_2/ZnO/TiO_2 NCs.

The sensing performance parameters such as sensitivity, LDR and DL of the RuO_2/ZnO/TiO_2 NC-based chlorobenzene sensor were estimated from the calibration curve of chlorobenzene concentrations *versus* response currents. To draw the calibration curve of CBZ sensor, the observed current density at different CBZ concentrations were isolated from Fig. 7(B) at a potential of +1.5 V and a new plot of current *versus* CBZ concentration was constructed, as illustrated in Fig. 8(A), known as the calibration curve of the CBZ sensor. As represented in Fig. 8(A), the current data were linear on the straight line over the concentration range of
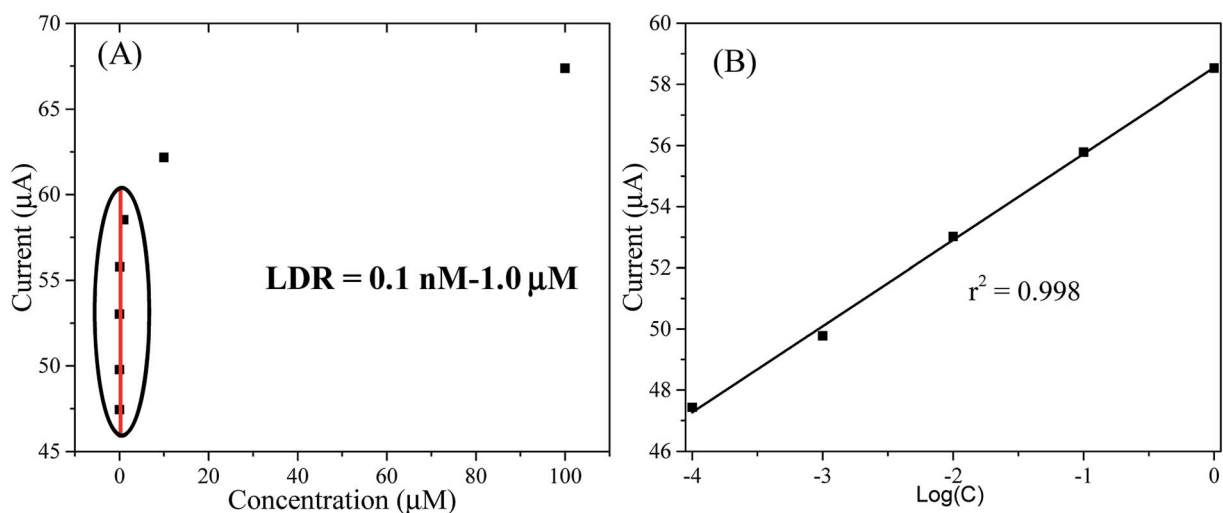

Fig. 8 (A) The calibration of the CBZ sensor based on the ternary RuO_2/ZnO/TiO_2 NCs/GCE, and (B) the linearity of LDR based on current *versus* log(CBZ concentration).

0.1 nM to 1 μM, which was denoted as the linear dynamic range (LDR) of the CBZ sensor. Obviously, the obtained LDR was very wider from 0.1 nM to 1.0 μM. To calculate the linearity (r^2) of LDR, current *versus* log(CBZ concentration) was plotted and presented in Fig. 8(B). The regression co-efficient r^2 was found to be 0.998, which demonstrated the good linearity of LDR. The CBZ sensor sensitivity was determined from the slope of the calibration curve by considering the area of the GCE (0.0316 cm^2). The obtained sensitivity result was calculated as 32.02 μA μM^{-1} cm^{-2}, which was the highest value compared to the reported articles on the CBZ sensor. The DL of CBZ sensor was calculated at a signal-to-noise ratio of 3 and the determined value was 98.7 ± 4.9 pM, which might be sufficiently low.

3.2.1. Optimization of the sensor. The reproducibility test of the CBZ sensor probe with RuO$_2$/ZnO/TiO$_2$ NCs/GCE was accomplished in 0.1 μM CBZ at an applied potential ranging from 0 to +1.5 V in a buffer medium of pH 7.0, as presented in Fig. 9(A). As represented in Fig. 9(A), there were no significant changes in the electrochemical responses of CBZs at successive

seven replicated runs. The obtained electrochemical responses were not altered on washing of the electrode after each run. Therefore, it can be predicted that the proposed sensor probe was stable-enough to generate similar electrochemical responses in the detection of CBZs under identical conditions. The response time is another key performance to measure the efficiency of the sensor and defined as the time required to achieve 90% of its steady stated signal.[95] To measure the response time, the electrodes of the proposed sensor were applied to analyze the CBZs at 0.1 μM at a pH of 7.0, as perceived in Fig. 9(B). As shown in Fig. 9(B), the current *versus* time plot becomes steady after 10 s. Therefore, the proposed CBZ sensor based on RuO$_2$/ZnO/TiO$_2$ NCs/GCE needed 10 s to complete the electrochemical response of CBZs and the response time was 9 s, which evidenced the high efficiency of the CBZ sensor.

Besides that, we analyzed the intra-day and inter-day electro-chemical responses with the RuO$_2$/ZnO/TiO$_2$ NCs/GCE sensor probe by an electrochemical method under identical conditions, as presented in Fig. 9(C and D). Seven readings were taken at 1 hour
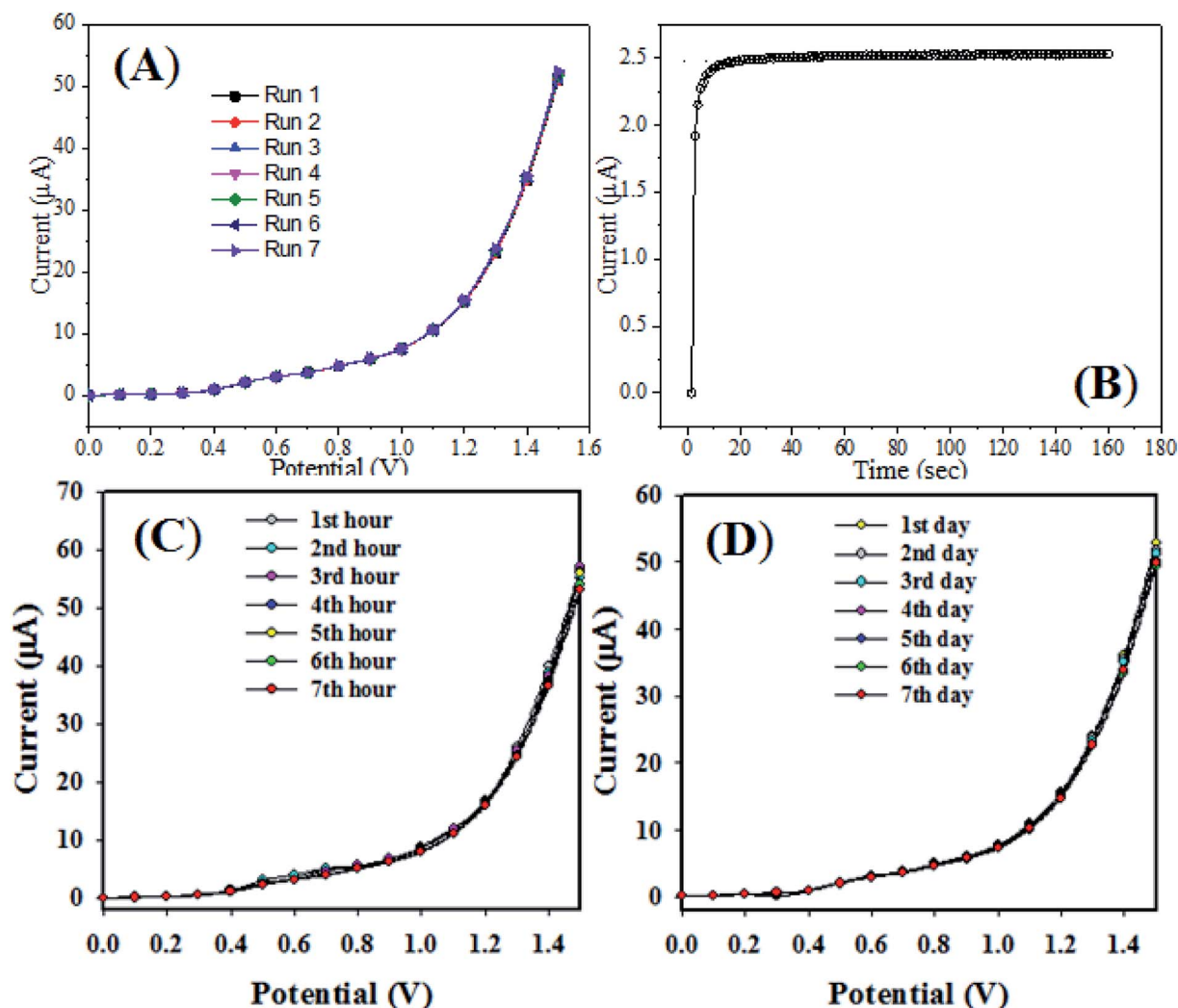

Fig. 9 Performance of reliability test: (A) reliability test of the CBZ sensor at 0.1 μM, (B) response time estimation, (C) intra-day reproducibility performances, and (D) inter-day reproducibility performances.
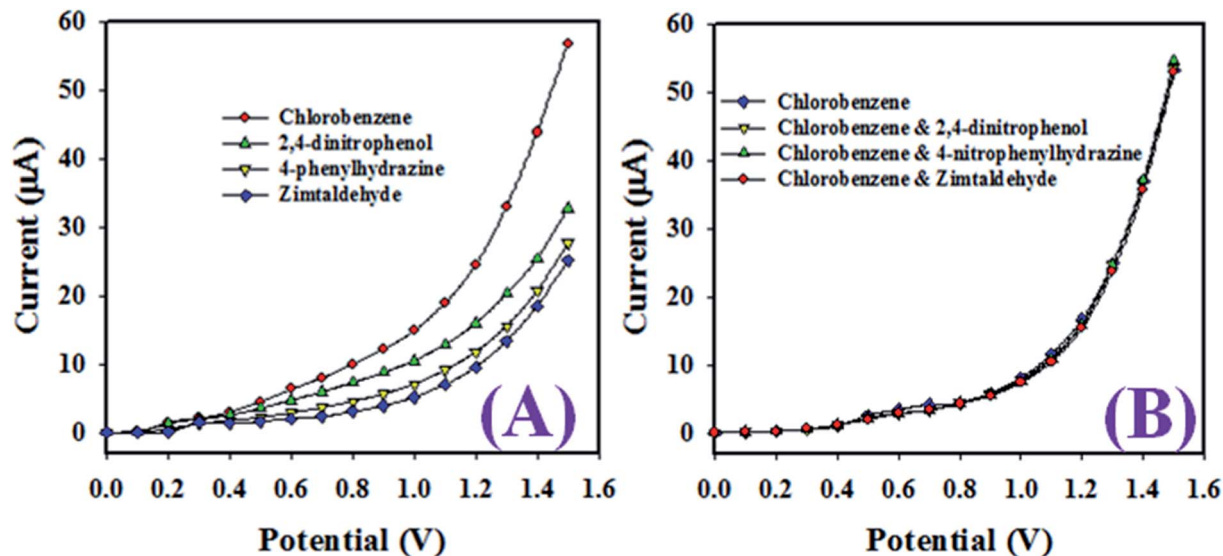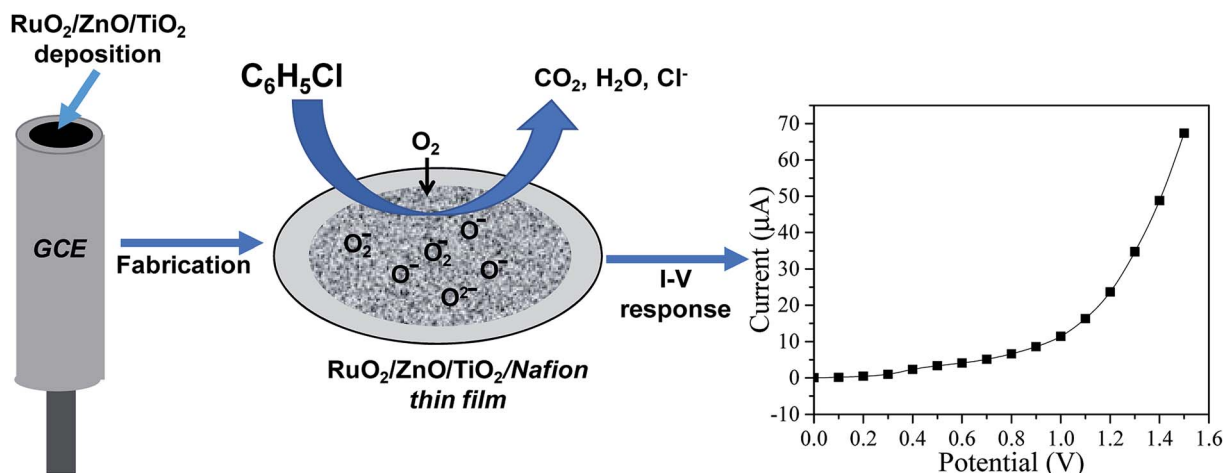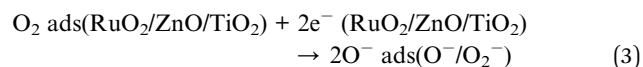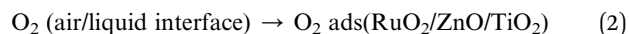
Fig. 10 (A) Electrochemical responses of various toxic chemicals at 0.1 μM concentration in a buffer phase of pH 7.0, and (B) interference effect of other co-existing toxins in the chlorobenzene sensor.

interval with the sensor probe for the detection of CBZs under identical conditions. However, the sensor reading was taken after one-day interval with the same electrode. The $RuO_2/ZnO/TiO_2$ NCs/ GCE sensor probe was very stable and almost reproducible, and stable responses were observed from these investigations.

As revealed in Fig. 10(A), the toxic chemicals such as CBZs, 2,4-dinitrophenol, 4-phenylhydrazine, and zimtaldehyde exhibited distinct electrochemical responses at 0.1 μM concentration in a buffer phase of pH 7.0. However, as shown in Fig. 10(B), the electrochemical responses of chlorobenzenes in the presence of 2,4-dinitrophenol, 4-phenylhydrazine, and zimtaldehyde were completely undistinguished and not possible to separate each other. Therefore, these investigations confirm that the projected sensor based on the ternary metal oxide $RuO_2/ZnO/TiO_2$ NCs/GCE was selective to

chlorobenzenes, and the other co-existing toxic chemicals did not alter its electrochemical response.

3.2.2. Sensing mechanism. The experimental results revealed that all the TiO_2, RuO_2/TiO_2 and ternary oxide $RuO_2/ZnO/TiO_2$ NC-based sensors were sensitive to CBZs. The response value of the sensor based on RuO_2/TiO_2 NPs was higher than the response value of TiO_2. Accordingly, the $RuO_2/ZnO/TiO_2$ NC-based electrochemical (EC) sensor demonstrated higher response current than TiO_2, RuO_2/TiO_2-based sensors. The possible sensing mechanism of the proposed sensor to detect CBZs is schematically shown in Scheme 1. The proposed mechanism could be explained with the following equations:

$$O_2 \text{ (air/liquid interface)} \rightarrow O_2 \text{ ads}(RuO_2/ZnO/TiO_2) \quad (2)$$

$$O_2 \text{ ads}(RuO_2/ZnO/TiO_2) + 2e^- \ (RuO_2/ZnO/TiO_2)$$
$$\rightarrow 2O^- \text{ ads}(O^-/O_2^-) \quad (3)$$

Scheme 1 Mechanism of CBZ detection with ternary oxide $RuO_2/ZnO/TiO_2$ NCs by an electrochemical approach in an aqueous medium.
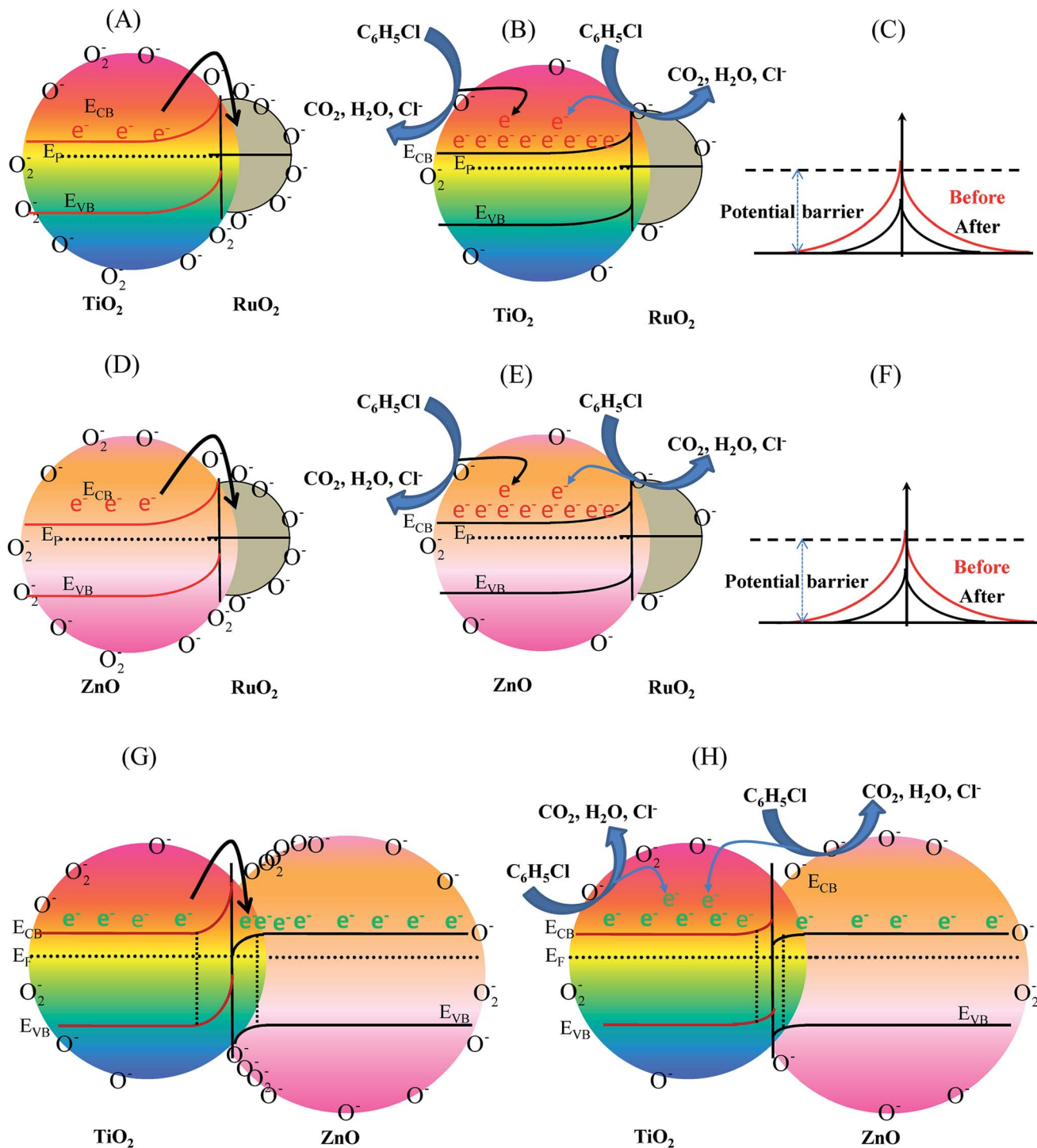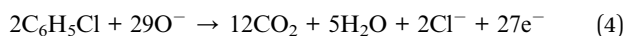
Fig. 11 Energy band diagram of nanocomposite systems when exposed to the CBZ solution; before (A) RuO_2/TiO_2, (D) RuO_2/ZnO, and (G) ZnO/TiO_2 and after: (B and C) RuO_2/TiO_2 (E and F) RuO_2/ZnO, and (H) ZnO/TiO_2.

$$2C_6H_5Cl + 29O^- \rightarrow 12CO_2 + 5H_2O + 2Cl^- + 27e^- \quad (4)$$

First of all, bulk oxygen molecules available at the liquid/air interface tended to adsorb and react with electrons from ternary $RuO_2/ZnO/TiO_2$ NC conduction bands, and subsequently, the

adsorbed oxygen was ionized (eqn (2) and (3)) and converted into negative oxygen species (O_2^-, O^-, O^{2-}) around the surface of ternary $RuO_2/ZnO/TiO_2$ NCs leading to an increase in the sensing material resistance. When CBZs reacted with the adsorbed oxygen species, they were oxidized as explained in eqn (4), liberating free electrons that were sent back to the

semiconductor conduction band. It is obvious from the above reactions that some of the chemisorbed O^- oxygen ions were removed for oxidizing CBZs, releasing electrons back to the semiconductor conduction band and increasing the electronic conductivity of the NP surface. The oxygen adsorption and the electrochemical CBZ oxidation were further confirmed by the preceding authors.[30,96,97]

The enhanced sensing mechanism of the ternary $RuO_2/ZnO/TiO_2$ NC-based EC sensor could be explained using the band theory of semiconductor metal oxides. First of all, the capture of electrons in the conduction band of both TiO_2 and ZnO by adsorbed oxygen led to the development of an electron-depleted, space-charge layer at the interface of ternary $RuO_2/ZnO/TiO_2$ NCs. Therefore, a potential barrier was built, which hindered the movement of the conduction band electron and increased the resistance of the sensing materials. Second, it is reported in our previous studies that the RuO_2 work function (6.2 eV) was larger than TiO_2 (3.8 eV) and ZnO (4.2 eV) work function.[69,98] Thus, the Fermi energy levels of both TiO_2 and ZnO were more negative than RuO_2. As a result, when RuO_2 came into contact with ZnO and TiO_2 NPs, the electrons migrated from TiO_2 and ZnO to RuO_2 for equalizing the Fermi levels at a thermal equilibrium, resulting in the development of an electron depletion region and surface upward bent band in the semiconductor (Fig. 11(A) and (D)).

The electron depletion region formed led to an internal electric field, resulting in increased resistance at the heterojunction. Third, the Fermi energy level (E_F) of TiO_2 was more negative than the Fermi energy level of ZnO;[69,98] electrons migrated from TiO_2 to ZnO until the Fermi level of the n–n heterojunction of ZnO/TiO_2 came to equilibrium. The migration of electrons to the ZnO side created an electron depletion layer on the side of TiO_2 and further bent the band and led to a higher resistance of sensing materials than the pure TiO_2 and ZnO sensors, as revealed in Fig. 11(G). Thus, at thermal equilibrium, the oxygen adsorption was enhanced on the ZnO surface because of the formation of an electron-enriched zone at the ZnO side. Furthermore, it led to a more substantial depletion of TiO_2 grains and the formation of contact potential at the interface of ZnO/TiO_2. According to the reaction mechanism as described above, when $RuO_2/ZnO/TiO_2$ NC-based sensors were exposed to chlorobenzenes, the interaction of CBZ molecules with pre-adsorbed oxygen ions released electrons back to the

conduction bands of the sensing $RuO_2/ZnO/TiO_2$ NCs. This significantly reduced the width of the depletion layer at the heterojunction of RuO_2/TiO_2 (Fig. 11(B and C)) and RuO_2/ZnO (Fig. 11(E and F)), and between TiO_2 and ZnO (Fig. 11(H)), resulting in a great decrease in sensor resistance, hence increasing the response current. In summary, the formation of heterojunctions in ternary $RuO_2/ZnO/TiO_2$ NCs greatly increased the resistance in the absence of CBZs and decreased the resistance in the presence of CBZs in comparison with the TiO_2 sensors. Furthermore, it is reported that nano-sized RuO_2 could act as a catalyst for the oxidation reaction.[99,100] As a catalyst for the oxidation reaction, RuO_2 activated the CBZ molecules when CBZs were adsorbed onto the RuO_2 surface. Subsequently, the activated CBZ molecules were migrated to react with oxygen species on the ZnO and TiO_2 metal oxide NP surface, thus releasing electrons and increasing the conductivity of the sensing materials. Consequently, the improved sensing activity of composite $RuO_2/ZnO/TiO_2$ NCs was ascribed to the combined effects of depleted layer formation at the surface of individual TiO_2 and ZnO and the formation of a hetero-junction between ZnO and TiO_2 grains and between RuO_2 and ZnO or TiO_2 grains.

To establish the reliability of this study, a comparison based on the analytical parameters of the CBZ sensor such as sensitivity, LDR and DL is illustrated in Table 1. It was found that the CBZ sensor based on $RuO_2/ZnO/TiO_2$ NCs/GCE exhibited better performances. As stated in Fig. 1, ternary oxide $RuO_2/ZnO/TiO_2$ NCs possessed high crystallinity with very small grain size at nano-levels. Besides this, the FESEM investigation confirmed that the synthesized nanomaterials consisted of nanoparticles with a spherical-like shape. Therefore, the reactive surface area of the synthesized NPs was very high. As a result, the prepared NPs on the GCE were able to provide a nano-environment, which was favorable for high electrochemical sensing performance. For these reasons, the assembled CBZ sensor exhibited better sensitivity, LDR and DL among the tested material, as illustrated in Table 1. Moreover, the projected CBZ sensor exhibited good reproducibility and efficiency in analyzing real environmental samples.

3.3. Analysis of real samples

To satisfy the real-time application of the proposed sensor, the presented CBZ sensor with $RuO_2/ZnO/TiO_2$ NCs/GCE was used

Table 1 Performance of the CBZ detection with various nanocomposite sensors by an electrochemical method[a]

Modified electrode	DL	LDR	Sensitivity	Ref.
FeO/CdO NCs/GCE	72.73 pM	0.089 nM to 0.89 mM	1.3054 $\mu A\ \mu M^{-1}\ cm^{-2}$	32
MCM-41/GCE	13.0 pM	0.089 nM to 8.9 mM	0.7468 $\mu A\ \mu M^{-1}\ cm^{-2}$	33
PPY/CZO/AgE	0.34 nM	0.35 nM to 3.5 mM	$2.702 \times 10^{-3}\ \mu A\ \mu M^{-1}\ cm^{-2}$	101
$RuO_2/ZnO/TiO_2$ NCs/GCE	98.7 pM	0.1 nM to 1.0 μM	32.02 $\mu A\ \mu M^{-1}\ cm^{-2}$	This work

[a] DL (detection limit), LDR (linear dynamic range).

Table 2 Measured concentrations of the CBZ analytes in real environmental samples

Sample	Added CBZ concentration (μM)	Determined CBZ concentration[a] by RuO$_2$/ZnO/TiO$_2$ NPs/GCE (μM)			Average recovery[b] (%)	RSD[c] (%) ($n = 3$)
		R1	R2	R3		
Industrial effluent	0.0100	0.0096	0.0095	0.0095	95.33	0.61
PC-baby bottle	0.0100	0.0098	0.0098	0.0099	98.33	0.59
PC-water bottle	0.0100	0.0103	0.0101	0.0098	100.66	2.50
PVC-FPB	0.0100	0.0101	0.0099	0.0102	100.67	1.52

[a] Mean of three repeated determination (signal to noise ratio 3) with by RuO$_2$/ZnO/TiO$_2$ NPs/GCE. [b] Concentration of CBZs determined/concentration taken (unit: μM). [c] Relative standard deviation value indicates precision among three repeated measurements (R1, R2, R3).

to detect CBZs in environmental samples applying a recovery method *via* an electrochemical approach. We used extracts of PC-baby bottle, industrial waste effluents, PC-water bottles, and PVC-food packaging bags (PVC-FPB) to measure CBZs in environmental samples. Based on the performance of the CBZ sensor, as indicated in Table 2, it was possible to detect the targeted analyte (CBZ) in the real environmental samples with acceptable and satisfactory results.

4. Conclusion

In conclusion, a highly sensitive CBZ sensor was developed based on ternary metal oxides such as RuO$_2$/ZnO/TiO$_2$ NCs on a GCE by an electrochemical approach. The RuO$_2$/ZnO/TiO$_2$ NC was prepared by an impregnation technique, while ZnO and TiO$_2$ NPs were synthesized by precipitation and sol–gel techniques, respectively. The sensor was assembled with a GCE modified with RuO$_2$/ZnO/TiO$_2$ NCs as a thin film with conducting Nafion binder, which served as the working electrode. The fabricated sensor showed good selectivity towards CBZ detection in a buffer medium compared to other chemicals. The response time was about 9 s, which was faster enough for real-time monitoring of sensor probes. The prepared NP sensor probe displays higher sensitivity, large LDR, lower DL, excellent reproducibility, good reliability and stability. At the end, the sensing mechanism of the ternary oxide RuO$_2$/ZnO/TiO$_2$-based electrochemical sensor was discussed and analyzed by the semiconductor energy-band theory in this report. This work provided a new strategy to utilize ternary metal oxide RuO$_2$/ZnO/TiO$_2$ NCs as efficient electron mediators to develop highly selective sensors toward CBZ detection for the safety of environmental and healthcare fields on large scales.

Conflicts of interest

On behalf of all authors, the corresponding author declares that there is no conflict of interest.

Acknowledgements

References

1 N. Kometani, S. Inata, A. Shimokawa and Y. Yonezawa, *Int. J. Photoenergy*, 2008, 512170, DOI: 10.1155/2008/512170.

2 K. Poplawski, J. Lichtenberger, F. J. Keil, K. Schnitzlein and M. D. Amiridis, *Catal. Today*, 2000, **62**(4), 329–336, DOI: 10.1016/S0920-5861(00)00434-X.

3 S. Krishnamoorthy, J. A. Rivas and M. D. Amiridis, *J. Catal.*, 2000, **193**(2), 264–272, DOI: 10.1006/jcat.2000.2895.

4 X. Ma, Q. Sun, X. Feng, X. He, J. Guo, H. Sun and H. Cao, *Appl. Catal., A*, 2013, **450**(15), 143–151, DOI: 10.1016/j.apcata.2012.10.019.

5 D. Calamari, S. Galassi, F. Setti and M. Vighi, *Chemosphere*, 1983, **12**(2), 253–262, DOI: 10.1016/0045-6535(83)90168-6.

6 Y. He, Y. Wang and H. K. Lee, *J. Chromatogr. A*, 2000, **874**, 149–154.

7 D. Djohan, J. Yu, D. Connell and E. Christensen, *J. Toxicol. Environ. Health, Part A*, 2007, **70**(19), 1594–1603, DOI: 10.1080/15287390701432384.

8 R. R. Kozani, Y. Assadi, F. Shemirani, M. R. M. Hosseini and M. R. Jamali, *Talanta*, 2007, **72**(2), 387–393, DOI: 10.1016/j.talanta.2006.10.039.

9 R. Nazari, L. Rajić, A. Ciblak, S. Hernández, I. E. Mousa, W. Zhou, D. Bhattacharyya and A. N. Alshawabkeh, *Chemosphere*, 2019, **226**, 556–563, DOI: 10.1016/j.chemosphere.2018.10.143.

10 L. S. Riter, L. Charles, M. Turowski and R. G. Cooks, *Rapid Commun. Mass Spectrom.*, 2001, **15**(23), 2290–2295, DOI: 10.1002/rcm.489.

11 P. Jandera, J. Fischer and B. Prokeš, *Chromatographia*, 2001, **54**, 581–587, DOI: 10.1007/BF02492182.

12 H. Borsdorf, A. Rämmler, D. Schulze, K. O. Boadu, B. Feist and H. Weiß, *Anal. Chim. Acta*, 2001, **440**, 63–70.

13 M. M. Alam, A. M. Asiri, M. M. Rahman and M. A. Islam, *Mater. Chem. Phys.*, 2020, **244**, 22740, DOI: 10.1016/j.matchemphys.2020.122740.

14 S. Vinoth, R. Ramaraj and A. Pandikumar, *Mater. Chem. Phys.*, 2020, **245**, 122743, DOI: 10.1016/j.matchemphys.2020.122743.

15 C. I. L. Justino, T. A. P. Rocha-Santos and A. C. Duarte, *TrAC, Trends Anal. Chem.*, 2013, **47**, 27–36, DOI: 10.1016/j.trac.2013.02.004.

16 M. T. Uddin, M. M. Alam, A. M. Asiri, M. M. Rahman, T. Toupance and M. A. Islam, *RSC Adv.*, 2020, **10**, 122–132, DOI: 10.1039/c9ra08669b.

17 M. M. Alam, A. M. Asiri and M. M. Rahman, *Mater. Chem. Phys.*, 2020, **243**, 122658, DOI: 10.1016/j.matchemphys.2020.122658.

18 P. Bollella, G. Fusco, C. Tortolini, G. Sanzò, G. Favero, L. Gorton and R. Antiochia, *Biosens. Bioelectron.*, 2017, **89**, 152–166, DOI: 10.1016/j.bios.2016.03.068.

19 Y. Song, Y. Luo, C. Zhu, H. Li, D. Du and Y. Lin, *Biosens. Bioelectron.*, 2016, **76**, 195–212, DOI: 10.1016/j.bios.2015.07.002.

20 R. C. Singh, O. Singh, M. P. Singh and P. S. Chandi, *Sens. Actuators, B*, 2008, **135**, 352–357, DOI: 10.1016/j.snb.2008.09.004.

21 M. K. Hossain, S. C. Ghosh, Y. Boontongkong, C. Thanachayanont and J. Dutta, *J. Metastable Nanocryst. Mater.*, 2005, **23**, 27–30, DOI: 10.4028/www.scientific.net/JMNM.23.27.

22 R. Jagadish, S. Yellappa, M. Mahanthappa and K. B. Chandrasekhar, *J. Chin. Chem. Soc.*, 2017, **64**, 813–821, DOI: 10.1002/jccs.201600817.

23 H. Ma, Y. Xu, Z. Rong, X. Cheng, S. Gao, X. Zhang, H. Zhao and L. Huo, *Sens. Actuators, B*, 2012, **174**, 325–331, DOI: 10.1016/j.snb.2012.08.073.

24 J. Huang, X. Xu, C. Gu, W. Wang, B. Geng, Y. Sun and J. Liu, *Sens. Actuators, B*, 2012, **173**, 599–606, DOI: 10.1016/j.snb.2012.07.068.

25 Z. Li, J. Li, L. Song, H. Gong and Q. Niu, *J. Mater. Chem. A*, 2013, **1**, 15377–15382, DOI: 10.1039/c3ta13500d.

26 C. Zhao, B. Huang, J. Zhou and E. Xie, *Phys. Chem. Chem. Phys.*, 2014, **16**, 19327–19332, DOI: 10.1039/c4cp02961e.

27 C. Gu, H. Huang, J. Huang, Z. Jin, H. Zheng, N. Liu, M. Li, J. Liu and F. Meng, *Sens. Actuators, A*, 2016, **252**, 96–103, DOI: 10.1016/j.sna.2016.11.004.

28 K. Li, Y. Luo, L. Gao, T. Li and G. Duan, *ACS Appl. Mater. Interfaces*, 2020, **12**, 16792–16804, DOI: 10.1021/acsami.0c00525.

29 Y. Tang and J. Ma, *RSC Adv.*, 2014, **4**, 25692–25697, DOI: 10.1039/c3ra46554c.

30 Z. Feng, C. Gao, X. Ma and J. Zhan, *RSC Adv.*, 2019, **9**, 42351–42359, DOI: 10.1039/c9ra09705h.

31 Y. Wan, J. Liu, W. Li, F. Meng, Z. Jin, X. Yu, X. Huang and J. Liu, *Nanotechnology*, 2011, **22**, 315501, DOI: 10.1088/0957-4484/22/31/315501.

32 M. M. Rahman, M. M. Alam and A. M. Asiri, *J. Ind. Eng. Chem.*, 2018, **62**, 392–400, DOI: 10.1016/j.jiec.2018.01.019.

33 B. M. Abu-Zied, M. M. Alam, A. M. Asiri, W. Schwieger and M. M. Rahman, *Colloids Surf., A*, 2019, **562**, 161–169, DOI: 10.1016/j.colsurfa.2018.11.024.

34 E. Comini, G. Faglia, G. Sberveglieri, Z. Pan and Z. L. Wang, *Appl. Phys. Lett.*, 2002, **81**, 1869–1871.

35 Ü. Özgür, Y. I. Alivov, C. Liu, A. Teke, M. A. Reshchikov, S. Doğan and V. Avrutin, *J. Appl. Phys.*, 2005, **98**, 041301.

36 M. Chakraborty, P. Mahapatra and R. Thangavel, *Thin Solid Films*, 2016, **612**, 49–54.

37 K. S. Lee, C. W. Park and J. D. Kim, *Colloids Surf., A*, 2017, **512**, 87–92.

38 R. Devi, M. Thakur and C. S. Pundir, *Biosens. Bioelectron.*, 2011, **26**, 3420–3426.

39 A. Umar, M. M. Rahman and Y.-B. Hahn, *J. Nanosci. Nanotechnol.*, 2009, **9**, 4686–4691.

40 H. B. Balkhoyor, M. M. Rahman and A. M. Asiri, *RSC Adv.*, 2016, **6**, 58236–58246, DOI: 10.1039/c6ra10863f.

41 H. Koga and T. Kitaoka, *Chem. Eng. J.*, 2011, **168**, 420–425.

42 K. Singh, A. A. Ibrahim, A. Umar, A. Kumar, G. R. Chaudhary, S. Singh and S. K. Mehta, *Sens. Actuators, B*, 2014, **202**, 1044–1050.

43 D. X. Ju, H. Y. Xu, Z. W. Qiu, Z. C. Zhang, Q. Xu, J. Zhang, J. Q. Wang and B. Q. Cao, *ACS Appl. Mater. Interfaces*, 215, **7**, 19163–19171, DOI: 10.1021/acsami.5b04904.

44 X. Song, Z. Wang, Y. Liu, C. Wang and L. Li, *Nanotechnology*, 2009, **20**, 075501, DOI: 10.1088/0957-4484/20/7/075501.

45 H. S. Woo, C. W. Na, I. D. Kim and J. H. Lee, *Nanotechnology*, 2012, **23**, 245501, DOI: 10.1088/0957-4484/23/24/245501.

46 C. S. Lee, I. D. Kim and J. H. Lee, *Sens. Actuators, B*, 2013, **181**, 463–470, DOI: 10.1016/j.snb.2013.02.008.

47 J. Zhao, F. Mu, L. Qin, X. Jia and C. Yang, *Mater. Chem. Phys.*, 2015, **166**, 176–181, DOI: 10.1016/j.matchemphys.2015.09.044.

48 X. Chen and S. S. Mao, *Chem. Rev.*, 2007, **107**(7), 2891–2959, DOI: 10.1021/cr0500535.

49 Y. Tang, P. Liu, J. Xu, L. Le Li, L. Yang, X. Liu, S. Liu and Y. Zhou, *Sens. Actuators, B*, 2018, **258**, 906–912, DOI: 10.1016/j.snb.2017.11.071.

50 E. Şennik, Z. Çolak, N. Kilinç and Z. Z. Öztürk, *Int. J. Hydrogen Energy*, 2010, **35**, 4420–4427, DOI: 10.1016/j.ijhydene.2010.01.100.

51 S. J. Bao, C. M. Li, J. F. Zang, X. Q. Cui, Y. Qiao and J. Guo, *Adv. Funct. Mater.*, 2008, **18**, 591–599, DOI: 10.1002/adfm.200700728.

52 S. Lin, D. Li, J. Wu, X. Li and S. A. Akbar, *Sens. Actuators, B*, 2011, **156**, 505–509, DOI: 10.1016/j.snb.2011.02.046.

53 H. C. Lee, L. F. Zhang, J. L. Lin, Y. L. Chin and T. P. Sun, *Sensors*, 2013, **13**, 14161–14174, DOI: 10.3390/s131014161.

54 J. Yu and H. Ju, *Anal. Chem.*, 2002, **74**, 3579–3583, DOI: 10.1021/ac011290k.

55 J. Yu and H. Ju, *Anal. Chim. Acta*, 2003, **486**, 209–216, DOI: 10.1016/S0003-2670(03)00508-7.

56 J. Riga, C. Tenret-Noel, J. J. Pireaux, R. Caudano and J. J. Verbist, *Phys. Scr.*, 1977, **16**, 351–354.

57 V. Subramanian, S. C. Hall, P. H. Smith and B. Rambabu, *Solid State Ionics*, 2004, **175**, 511–515, DOI: 10.1016/j.ssi.2004.01.070.

58 E. R. Kötz and S. Stucki, *J. Appl. Electrochem.*, 1987, **17**, 1190–1197.

59 A. Mills, P. A. Duckmanton and J. Reglinski, *Chem. Commun.*, 2010, **46**, 2397.

60 K. Reuter and M. Scheffler, *Phys. Rev. B: Condens. Matter Mater. Phys.*, 2006, **73**, 045433.

61 N. López, J. Gómez-Segura, R. P. Marín and J. Pérez-Ramírez, *J. Catal.*, 2008, **255**, 29–39.

62 C. Mondelli, A. P. Amrute, F. Krumeich, T. Schmidt, J. Perez-Ramirez and J. Pérez-Ramírez, *ChemCatChem*, 2011, **3**, 657–660.

63 M. M. Rahman, J. Ahmed and A. M. Asiri, *Biosens. Bioelectron.*, 2018, **99**, 586–592, DOI: 10.1016/j.bios.2017.08.039.

64 M. M. Alam, A. M. Asiri, M. M. Rahman and M. A. Islam, *Surf. Interfaces*, 2020, **19**, 100540, DOI: 10.1016/j.surfin.2020.100540.

65 J. Ahmed, M. M. Rahman, I. A. Siddiquey, A. M. Asiri and M. A. Hasnat, *Sens. Actuators, B*, 2018, **256**, 383–392, DOI: 10.1016/j.snb.2017.10.076.

66 M. M. Alam, M. M. Rahman, M. T. Uddin, A. M. Asiri, Inamuddin, M. T. Saeed Chani and M. A. Islam, *J. Lumin.*, 2020, **227**, 117528, DOI: 10.1016/j.jlumin.2020.117528.

67 M. M. Rahman and J. Ahmed, *Biosens. Bioelectron.*, 2018, **102**, 631–636.

68 M. T. Uddin, Y. Nicolas, C. Olivier, W. Jaegermann, N. Rockstroh, H. Junge and T. Toupance, *Phys. Chem. Chem. Phys.*, 2017, **19**, 19279–19288, DOI: 10.1039/c7cp01300k.

69 M. T. Uddin, Y. Nicolas, C. Olivier, T. Toupance, M. M. Müller, H. J. Kleebe, K. Rachut, J. Ziegler, A. Klein and W. Jaegermann, *J. Phys. Chem. C*, 2013, **117**, 22098–22110, DOI: 10.1021/jp407539c.

70 T. Sreethawong, Y. Yamada, T. Kobayashi and S. Yoshikawa, *J. Mol. Catal. A: Chem.*, 2005, **241**, 23–32, DOI: 10.1016/j.molcata.2005.07.009.

71 M. T. Uddin, Y. Nicolas, C. Olivier, W. Jaegermann, N. Rockstroh, H. Junge and T. Toupance, *Phys. Chem. Chem. Phys.*, 2017, **19**, 19279–19288, DOI: 10.1039/c7cp01300k.

72 Y. Zhang, F. Zhu, J. Zhang and L. Xia, *Nanoscale Res. Lett.*, 2008, **3**, 201–204.

73 M. T. Uddin, Y. Nicolas, C. Olivier, L. Servant, T. Toupance, S. Li, A. Klein and W. Jaegermann, *Phys. Chem. Chem. Phys.*, 2015, **17**, 5090–5102, DOI: 10.1039/c4cp04780j.

74 A. L. Patterson, *Phys. Rev.*, 1939, **56**, 978, DOI: 10.1103/PhysRev.56.978.

75 V. Bilovol, S. Ferrari, D. Derewnicka and F. D. Saccone, *Mater. Chem. Phys.*, 2014, **146**, 269–276, DOI: 10.1016/j.matchemphys.2014.03.021.

76 M. C. Biesinger, L. W. M. Lau, A. R. Gerson and R. S. C. Smart, *Appl. Surf. Sci.*, 2010, **257**, 887–898, DOI: 10.1016/j.apsusc.2010.07.086.

77 M. Pérez-González and S. A. Tomás, *Catal. Today*, 2019, DOI: 10.1016/j.cattod.2019.08.009.

78 D. Briggs, C. D. Wanger, W. M. Riggs, L. E. Davis, J. F. Moulder and G. E. Muilenberg, *Handbook of X-ray Photoelectron Spectroscopy: a reference book of standard data for use in x-ray photoelectron spectroscopy*, PerkinElmer Corp, 1979.

79 S. Parthasarathy, V. Nandhini and B. G. Jeyaprakash, *J. Colloid Interface Sci.*, 2016, **482**, 81–88, DOI: 10.1016/j.jcis.2016.07.066.

80 Y. Kaga, Y. Abe, H. Yanagisawa, M. Kawamura and K. Sasaki, *Surf. Sci. Spectra*, 1999, **6**, 68–74, DOI: 10.1116/1.1247890.

81 P. Banerjee, W. J. Lee, K. R. Bae, S. B. Lee and G. W. Rubloff, *J. Appl. Phys.*, 2010, **108**, 043504.

82 A. Ievtushenko, O. Khyzhun, I. Shtepliuk, V. Tkach, V. Lazorenko and G. Lashkarev, *Acta Phys. Pol., A*, 2013, **124**, 858–861, DOI: 10.12693/APhysPolA.124.858.

83 M. T. Uddin, O. Babot, L. Thomas, C. Olivier, M. Redaelli, M. D'Arienzo, F. Morazzoni, W. Jaegermann, N. Rockstroh, H. Junge and T. Toupance, *J. Phys. Chem. C*, 2015, **119**, 7006–7015, DOI: 10.1021/jp512769u.

84 Y. Zhan, M. R. J. Tan, X. Cheng, W. M. A. Tan, G. F. Cai, J. W. Chen, V. Kumar, S. Magdassi and P. S. Lee, *J. Mater. Chem. C*, 2017, **5**, 9995–10000, DOI: 10.1039/c7tc02456h.

85 G. G. Guillén, M. I. M. Palma, B. Krishnan, D. Avellaneda, G. A. Castillo, T. K. D. Roy and S. Shaji, *Mater. Chem. Phys.*, 2015, **162**, 561–570, DOI: 10.1016/j.matchemphys.2015.06.030.

86 J. P. Zhao, W. Y. Hernández, W. J. Zhou, Y. Yang, E. I. Vovk, M. Capron and V. Ordomsky, *ChemCatChem*, 2020, **12**, 238–247, DOI: 10.1002/cctc.201901249.

87 E. A. Davis and N. F. Mott, *Philos. Mag.*, 1970, **22**, 0903–0922, DOI: 10.1080/14786437008221061.

88 E. Sanchez and T. Lopez, *Mater. Lett.*, 1995, **25**, 271–275, DOI: 10.1016/0167-577X(95)00190-5.

89 A. B. Murphy, *Sol. Energy Mater. Sol. Cells*, 2007, **91**, 1326–1337, DOI: 10.1016/j.solmat.2007.05.005.

90 M. M. Alam, M. T. Uddin, A. M. Asiri, M. M. Rahman and M. A. Islam, *Measurement*, 2020, **163**, 107990, DOI: 10.1016/j.measurement.2020.107990.

91 M. M. Rahman, M. M. Alam, A. M. Asiri and M. A. Islam, *Talanta*, 2017, **170**, 215–223, DOI: 10.1016/j.talanta.2017.04.017.

92 M. M. Alam, A. M. Asiri, M. T. Uddin, M. A. Islam and M. M. Rahman, *ChemistrySelect*, 2018, **3**, 11460–11468, DOI: 10.1002/slct.201802750.

93 M. M. Alam, A. M. Asiri, M. T. Uddin, M. A. Islam and M. M. Rahman, *RSC Adv.*, 2018, **8**, 12562–12572, DOI: 10.1039/c8ra01734d.

94 M. M. Alam, A. M. Asiri, M. T. Uddin, M. A. Islam, M. R. Awual and M. M. Rahman, *New J. Chem.*, 2019, **43**, 8651–8659, DOI: 10.1039/c9nj01287g.

95 A. Wei, L. Pan and W. Huang, *Mater. Sci. Eng., B*, 2011, **176**, 1409–1421, DOI: 10.1016/j.mseb.2011.09.005.

96 G. N. Dar, A. Umar, S. A. Zaidi, S. Baskoutas, S. H. Kim, M. Abaker, A. Al-Hajry and S. A. Al-Sayari, *Sci. Adv. Mater.*, 2011, **3**, 901–906, DOI: 10.1166/sam.2011.1242.

97 M. Abaker, A. Umar, S. Baskoutas, G. N. Dar, S. A. Zaidi, S. A. Al-Sayari, A. Al-Hajry, S. H. Kim and S. W. Hwang, *J. Phys. D: Appl. Phys.*, 2011, **44**, 425401, DOI: 10.1088/0022-3727/44/42/425401.

98 M. T. Uddin, Y. Nicolas, C. Olivier, L. Servant, T. Toupance, S. Li, A. Klein and W. Jaegermann, *Phys. Chem. Chem. Phys.*, 2015, **17**, 5090–5102.

99 J. Lim, J. M. Lee, C. Kim, S. J. Hwang, J. Lee and W. Choi, *Environ. Sci.: Nano*, 2019, **6**, 2084–2093, DOI: 10.1039/c9en00500e.

100 R. He, G. Xu, Y. Wu, K. Shi, H. Tang, P. Ma, J. Zeng, Y. Bai and S. Chen, *Int. J. Hydrogen Energy*, 2019, **44**, 5940–5947, DOI: 10.1016/j.ijhydene.2019.01.114.

101 A. A. P. Khan, A. Khan, M. M. Rahman, A. M. Asiri and M. Oves, *Int. J. Biol. Macromol.*, 2017, **98**, 256–267, DOI: 10.1016/j.ijbiomac.2017.02.005.